

# Improved Biocompatibility of Amino-Functionalized Graphene Oxide in *Caenorhabditis elegans*

Corvin Rive, Giacomo Reina, Prerana Wagle, Emanuele Treossi, Vincenzo Palermo, Alberto Bianco, Lucia Gemma Delogu, Matthias Rieckher,\* and Björn Schumacher\*

Graphene oxide (GO) holds high promise for diagnostic and therapeutic applications in nanomedicine but reportedly displays immunotoxicity, underlining the need for developing functionalized GO with improved biocompatibility. This study describes adverse effects of GO and amino-functionalized GO (GONH<sub>2</sub>) during *Caenorhabditis elegans* development and ageing upon acute or chronic exposure. Chronic GO treatment throughout the *C. elegans* development causes decreased fecundity and a reduction of animal size, while acute treatment does not lead to any measurable physiological decline. However, RNA-Sequencing data reveal that acute GO exposure induces innate immune gene expression. The p38 MAP kinase, PMK-1, which is a well-established master regulator of innate immunity, protects *C. elegans* from chronic GO toxicity, as *pmk-1* mutants show reduced tissue-functionality and facultative vivipary. In a direct comparison, GONH<sub>2</sub> exposure does not cause detrimental effects in the wild type or in *pmk-1* mutants, and the innate immune response is considerably less pronounced. This work establishes enhanced biocompatibility of amino-functionalized GO in a whole-organism, emphasizing its potential as a biomedical nanomaterial.

and specifically its derivative graphene oxide (GO), is poised to play a central role in the future of nanomedicine, as it combines a number of advantageous chemical properties, including a large surface area that can be easily functionalized, high chemical stability, amphiphaticity, and high thermal and electric conduction. Hence, GO holds great promise to be employable for drug delivery, tissue-engineering, biomedical imaging and diagnostics in human disease.<sup>[4,5]</sup> A rising number of recent studies focuses on the design of GO, GO composites, or functionalized GO, and their application in anticancer drug delivery, tumor detection, and ablation of cancerous tissue.<sup>[6–11]</sup> Importantly, there is indication that few layer graphene directly triggers necrotic cell death in monocytic cancer cells through an unknown mode-of-action, while other cell populations stay unharmed.<sup>[12]</sup>

In this context, the question about toxicity and immune compatibility becomes central


for future nanomedical applications of graphene-based materials including GO, which has been addressed in an increasing amount of studies.<sup>[13]</sup> When injected into the blood stream, or administered through the airway, acute GO exposure at high doses can cause pulmonary inflammation, cardiovascular and systemic toxicity in mice and rats.<sup>[14]</sup> GO can also adversely affect fecundity; some studies report toxicity to germ cells and reduced fertility in

## 1. Introduction

The advent of nanotechnology has advanced the development of innovative biomedical research tools and therapeutic clinical applications in nanomedicine.<sup>[1,2]</sup> Graphene is a unique nanomaterial that is defined as a flat monolayer of carbon atoms, which are organized into a 2D honeycomb sp<sup>2</sup> lattice.<sup>[3]</sup> Graphene,

C. Rive, Dr. M. Rieckher, Prof. B. Schumacher  
Institute for Genome Stability in Ageing and Disease  
Medical Faculty  
University of Cologne  
Joseph-Stelzmann-Str. 26, 50931 Cologne, Germany  
E-mail: mriekch1@uni-koeln.de; bjoern.schumacher@uni-koeln.de

C. Rive, P. Wagle, Dr. M. Rieckher, Prof. B. Schumacher  
Cologne Excellence Cluster for Cellular Stress Responses  
in Ageing-Associated Diseases (CECAD)  
Center for Molecular Medicine Cologne (CMMC)  
University of Cologne  
Joseph-Stelzmann-Str. 26, 50931 Cologne, Germany

 The ORCID identification number(s) for the author(s) of this article can be found under <https://doi.org/10.1002/sml.201902699>.

© 2019 The Authors. Published by WILEY-VCH Verlag GmbH & Co. KGaA, Weinheim. This is an open access article under the terms of the Creative Commons Attribution-NonCommercial License, which permits use, distribution and reproduction in any medium, provided the original work is properly cited and is not used for commercial purposes.

DOI: 10.1002/sml.201902699

Dr. G. Reina, Prof. A. Bianco  
University of Strasbourg  
CNRS  
Immunology  
Immunopathology and Therapeutic Chemistry  
UPR 3572, 67000 Strasbourg, France

Dr. E. Treossi, Dr. V. Palermo  
ISOF-CNR  
via Gobetti 101, 40129 Bologna, Italy

Dr. L. G. Delogu  
University of Sassari  
via Muroni 23, 07100 Sassari, Italy

Dr. L. G. Delogu  
Institute of Pediatric Research  
Fondazione Città della Speranza  
corso stati uniti 4, 35127 Padua, Italy

Dr. L. G. Delogu  
Department of Biomedical Sciences  
University of Padua  
via Ugo bassi 58, 35121 Padua, Italy

male mice that might depend on elevated cellular reactive oxygen species contents and subsequent DNA damage induction that in turn triggers apoptosis.<sup>[15,16]</sup> Accordingly, GO exposure can cause an immune response, involving the activation of macrophages and various interleukins, as well as neutrophil extracellular trap formation similar to pathogen exposure.<sup>[17–19]</sup> The degree of toxicity and immune response activation that is observed across studies depend on the GO synthesis protocol and the resulting variability of physicochemical properties, which is determined by the lateral sheet size, vacancy or lattice defects, chemical purity and specific surface functionalization.<sup>[13,20–22]</sup> In cell culture, surface functionalization or coating with organic compounds, or metals, has been shown to improve GO biocompatibility by reducing toxicity and immune response activation.<sup>[23–25]</sup> Single-cell mass cytometry combined with whole-transcriptomic analysis revealed that amino-functionalized GO (GONH<sub>2</sub>) causes reduced metabolic perturbations in immune cells when compared to GO.<sup>[26]</sup> However, it remains unknown, whether GO or GONH<sub>2</sub> treatment might adversely affect a whole-organism.

The genetically tractable nematode *C. elegans* has proven to be an informative model when it comes to understanding the mode-of-actions and toxicity of organic compounds or nanomaterials.<sup>[27–29]</sup> Stress response mechanisms, including signaling pathways that regulate the innate immune response, are well-conserved in *C. elegans*, and protect the animals from environmental stress, pathogens, viruses, toxins and heavy metals, making the worm a powerful model for complex human diseases.<sup>[30,31]</sup> In recent years, the possible adverse effects of graphene on *C. elegans* have been investigated, resulting in considerable variations between the studies when measuring fecundity, development and lifespan, which might depend on the differences between the GO synthesis protocols and the specific treatment paradigm.<sup>[32–35]</sup>

In this work, we exposed *C. elegans* to small size GO and derived GONH<sub>2</sub> under two regimens: acute (12 h) and chronic treatment (72 h). We characterized fecundity, developmental timing, physiology and lifespan, and found comparatively mild adverse effects upon chronic GO exposure, which were not detected upon exposure to amino-functionalized graphene oxide. Further, we performed RNA-Seq of whole-animal populations to resolve the response on a transcriptome-level upon acute GO treatment and found a mild but significant upregulation of the innate immune response, which was less pronounced upon GONH<sub>2</sub>. The response to GO depends on the conserved PMK-1 p38 MAP kinase pathway that governs the innate immune response in the nematode. The adverse effects caused by graphene could be suppressed upon genetic germline depletion in *C. elegans*. Overall, our study provides evidence that GO exposure causes systemic physiological damage, when combined with other genetic and environmental stressors, which is robustly reduced when exposed to amino-functionalized graphene.

## 2. Results

### 2.1. GO Synthesis and Characterization

Graphene oxide was synthesized via a modified Hummers' method. The starting solution (2.5 g L<sup>-1</sup>) was then sonicated for 40 h and diluted to reach the desired concentrations.<sup>[36]</sup>

The obtained GO has a size of 124±26 nm, calculated from the analysis of atomic force microscopy (AFM) images (Figure S1A,B, Supporting Information). Subsequently, amino-functionalized GO was prepared by epoxide ring opening, as previously described.<sup>[37]</sup> Briefly, 2,2-(ethylenedioxy)bis(ethylamine) was grafted onto the sheets to form amino-functionalized GONH<sub>2</sub>. This amination reaction was performed in mild conditions and in water to avoid any undesired effect of organic solvents. To remove the unreacted diamine, GONH<sub>2</sub> was purified gently through extensive dialysis. Transmission electron microscopy (TEM) of GONH<sub>2</sub> shows that the morphology and the lateral size of the nanosheets is preserved (Figure S1C, Supporting Information). Additionally, little agglomeration was found in the case of GONH<sub>2</sub> flakes. Fourier-transform infrared spectroscopy (FTIR) characterization of GO displays the typical broad band of the OH stretching at 3370 cm<sup>-1</sup>, and two sharp bands at 1708 and 1625 cm<sup>-1</sup> attributed to the carbonyl and C=C stretching, respectively (Figure S1D, Supporting Information). The functionalization clearly modified the infrared spectrum of the material. The N–H stretching bands at 3370 and 3220 cm<sup>-1</sup> overlap with the OH stretching. In addition, the band at 1625 cm<sup>-1</sup> appears more intense together with the band at 1078 cm<sup>-1</sup>, corresponding to the N–H bending and C–N stretching, respectively. The new bands visible at 2910 and 1360 cm<sup>-1</sup> have been associated with the CH<sub>2</sub> stretching and bending, respectively. Thermogravimetric profile of GO (Figure S1E, Supporting Information) shows a typical trend with a first mass loss below 100 °C ascribed to the desorption of adsorbed water and unstable oxygenated groups, a second loss around 200 °C due to the decomposition of more stable oxygenated groups.<sup>[37]</sup> GONH<sub>2</sub> presents a less significant thermal loss, which has been attributed to the instability of some oxygenated group present on the GO surface that are depleted during the amination reaction.<sup>[38]</sup> The Kaiser test confirmed the presence of free amines on the GO surface. Amination reaction produced the increase of the percentage of nitrogen from 0.59 ± 0.03 for GO to 3.2 ± 0.2 for GONH<sub>2</sub> as atomic N%, which was assessed by X-Ray photoelectron spectroscopy (XPS).

### 2.2. Effects of GO on *C. elegans* Physiology

We designed two treatment paradigms to expose wild type *C. elegans* with GO flakes, or GONH<sub>2</sub>: acute treatment, which was applied from the larval stage 4 (L4) to young adulthood (12 h), and chronic treatment that started at L1 of development until day 1 of adulthood (72 h; see the Experimental Section; Figure 1A). We performed initial tests using 1, 10, 100, and 200 µg mL<sup>-1</sup> concentration of GO and GONH<sub>2</sub> acute treatments but initial assessment did not reveal any adverse effects on animal development, morphology, offspring number or movement on plates (data not shown). However, chronic GO treatments at 100 and 200 µg mL<sup>-1</sup> led to an obvious size difference and reduced brood size. For a quantitative analysis we focused on the concentration of 100 µg mL<sup>-1</sup> thereon.

The *C. elegans* germline commences proliferation of the somatic gonad and the germ cells at mid-L1 stage until a fully functional germline is established in adults, finalizing in the production of ≈300 offspring.<sup>[39]</sup> Adverse effects on egg laying

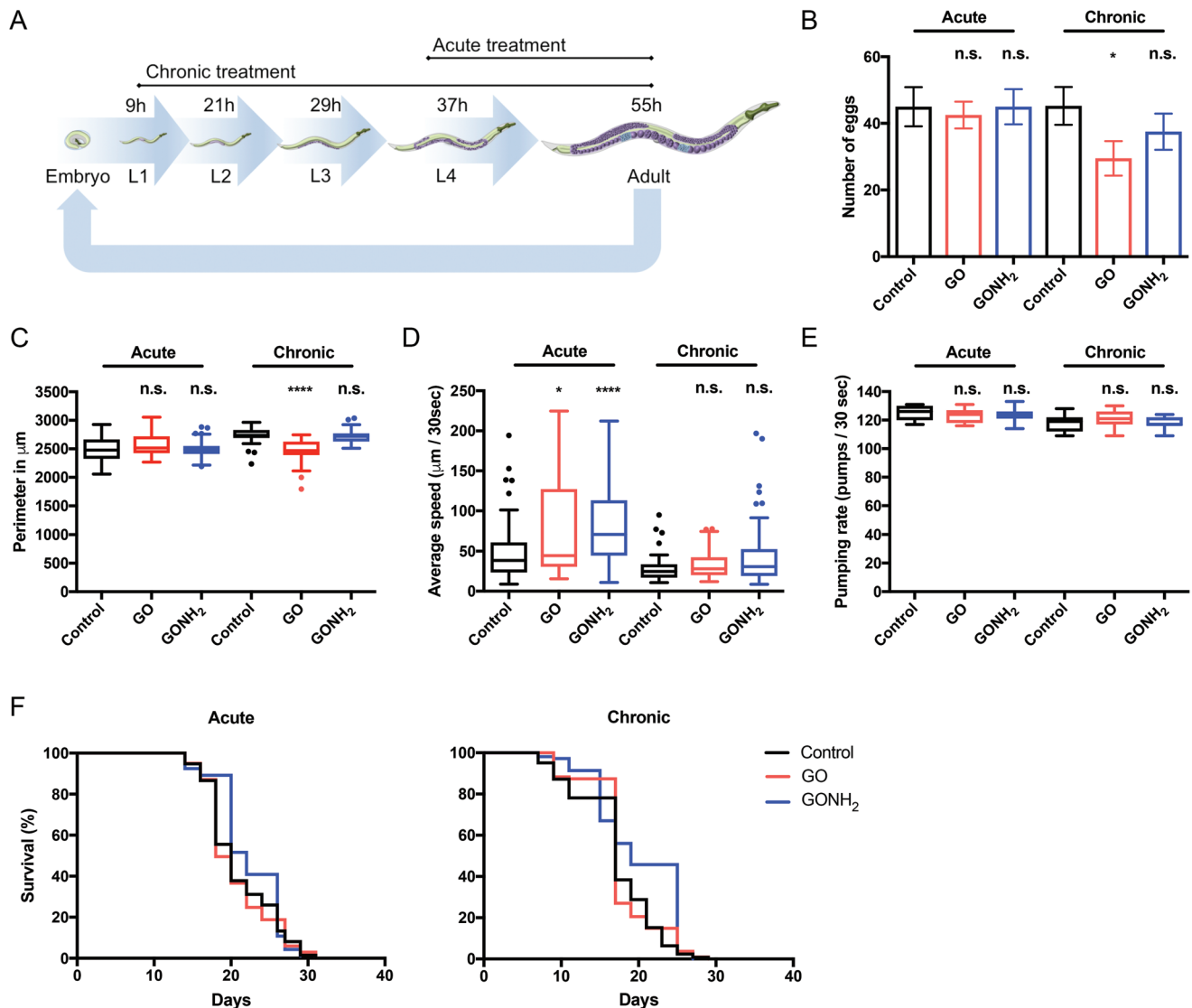


**Figure 1.** The effects of GO or GONH<sub>2</sub> upon acute or chronic exposure. All experiments were performed at 20 °C. A) Developmental timing of *C. elegans* (at 20 °C) and the two treatment paradigms used in this study. Acute treatment was performed from mid-L4 stage to young adults (12 h), while chronic treatment was performed from L1 stage to 1 d adults (72 h). B) Egg-laying measurement. Significance against the control was determined by the unpaired *t*-test, with \**p* < 0.05. Chronic GO treatment reduced wild type egg-laying in two out of three experiments. C) Size measurement (perimeter). Statistical analysis was performed by using the Mann–Whitney test with \*\*\*\**p* < 0.0001. Outliers are displayed according to the Tukey test (connected Figure S2, Supporting Information). D) Locomotion measurement. Significance test via Mann–Whitney analysis, with \**p* < 0.05, \*\*\*\**p* < 0.0001. Outliers are displayed according to the Tukey analysis. E) Pumping rates of animals after acute or chronic treatment. Significance was determined via the unpaired Mann–Whitney test, in comparison to the control, respectively. F) Representative lifespan graphs for acute versus chronic treatment (connected Table S1, Supporting Information).

and hatching rates can be indicative of defects in somatic gonad development, or damage to the germ cells, oocytes or the developing embryo.<sup>[40]</sup> Indeed, chronic GO treatment resulted in a significantly reduced egg-laying rate, which was not observed in the acute treatment regime or upon exposure to GONH<sub>2</sub> (Figure 1B). The hatching rate was 100% in all treatments (data not shown). Chronic treatment with GO resulted in decreased animal size, which was not the case upon GONH<sub>2</sub> exposure (Figure 1C). The size differences prompted us to investigate animal development in greater detail. Developmental timing is tightly regulated and highly reproducible in *C. elegans*, and the different developmental

stages, from the embryo, through the four larval stages (L1 to L4) to adults (Figure 1A), are easily quantified at the stereoscope.<sup>[40]</sup> The analysis of animal development at 24, 48, and 72 h time points did not reveal any significant differences after chronic exposure (Figure S2, Supporting Information).

We continued our analysis by quantifying post-developmental somatic phenotypes, including locomotion, pharyngeal pumping rates and longevity (Figure 1D–F). We applied worm-tracking software to analyze recordings of animal movement<sup>[41]</sup> after acute treatment with GO or GONH<sub>2</sub>, and determined that the average speed of animals roaming on the plate was

significantly increased, which was not observed upon chronic treatment (Figure 1D). We quantified the pumping rate of the pharynx, which is the feeding apparatus in *C. elegans* that is controlled by neuro-muscular activity.<sup>[42]</sup> None of the treatment paradigms significantly affected pharyngeal pumping behavior (Figure 1E). The nematode is a well-established model system to study the genetic and molecular mechanisms of the ageing process.<sup>[43]</sup> We monitored lifespan after acute or chronic treatment and found that GO exposure did not significantly influence longevity. However, in every second experiment we detected a small but significant lifespan extension in animals that were treated with GONH<sub>2</sub> (Figure 1F; 1 out of 2 experiments in acute treatment, 2 out of 4 experiments in chronic treatment), while the accumulated summary of all experiments did not show a significant difference between treatments (Table S1, Supporting Information).

Taken together, our results indicate that chronic GO exposure throughout the developmental process of *C. elegans* can lead to adverse effects on fecundity and animal size, which are not observed upon treatment with functionalized GONH<sub>2</sub>. Acute treatment does not result in a significant decline in any of the measured behavioral readouts.

### 2.3. Acute GO Exposure Results in a Transcriptional Induction of Genes Acting in the Innate Immune Response

To assess the effects of graphene on gene expression we performed RNA-Seq for transcriptome profiling upon acute treatment with GO or GONH<sub>2</sub> (see the Experimental Section). In total, 231 genes were differentially regulated ( $FC \geq \pm 1.2$ ) upon GO exposure, while GONH<sub>2</sub> affected the expression levels of 89 genes, and 83 genes were similarly affected by exposure to either material (Figure 2A; Tables S2 and S3, Supporting Information). We identified that differential expression of genes that act in innate immunity, or in the defense response to gram-negative or gram-positive bacteria was overrepresented upon GO treatment (at least 55 genes), and to a lesser extend upon exposure to GONH<sub>2</sub> (20 genes; Figure 2B,C). Analysis of the data sets showed that the fold changes in expression levels were relatively small but the differential expression was highly significant across replicates (Figure 2C). We validated gene expression levels by reverse transcriptase-quantitative polymerase chain reaction (RT-qPCR), focusing on a subset of innate immunity genes, which were differentially changed in both GO and GONH<sub>2</sub> RNA-sequencing (RNA-Seq) data sets (Figure S3, Tables S4 and S5, Supporting Information).

The significant differential regulation of innate immunity genes upon GO treatment prompted us to investigate a possible correlation to previously obtained gene expression data sets on pathogen infection in *C. elegans*. The nematode is a well-established model to study host-pathogen interaction and the effects on organismal stress responses and innate immunity.<sup>[30,44]</sup> Exposure to the human opportunistic pathogen *Pseudomonas aeruginosa* (PA14) causes a strong PMK-1 dependent transcriptional response that correlates with gene expression changes caused by other pathogens, bacterial toxins or heavy metals.<sup>[45]</sup> Based on our RNA-Seq data, genes that have significantly altered gene expression upon GO treatment show a significant positive Pearson product-moment correlation with genes that

are differentially expressed upon PA14 exposure ( $r = 0.2719412$ ,  $p = 2.196 \times 10^{-7}$ ; Figure 2D). The correlation of data obtained from GONH<sub>2</sub>-exposed animals with PA14 treatment-derived data was less pronounced, and less significant ( $r = 0.1462944$ ,  $p = 0.006036$ ; Figure 2D). Together, the RNA-Seq analysis shows that GO triggers a, compared to pathogen infection, relatively mild, but highly significant induction of innate immune gene expression, which is further reduced upon exposure to GONH<sub>2</sub>.

### 2.4. Innate Immune Defects Increase Sensitivity to GO Exposure

The innate immune response to a variety of pathogens in *C. elegans* is governed by the activity of the PMK-1 p38 MAP kinase pathway.<sup>[46]</sup> Parallel functions in pathogen resistance have been described for the MPK-1 ERK MAP kinase pathway and the mammalian hormone receptor homolog FSHR-1, amongst others.<sup>[47,48]</sup> Based on the observation that the innate immune response was transcriptionally activated upon graphene exposure (Figure 2), we exposed *pmk-1*, *mpk-1*, and *fshr-1* deficient animals chronically to GO or GONH<sub>2</sub> and assessed the pumping rates. Loss of *pmk-1* resulted in a significant reduction of pumping behaviour upon GO exposure, while *mpk-1* and *fshr-1* mutants were unaffected (Figure S4A, Supporting Information).

In addition to its prominent role in pathogen defense, PMK-1 also responds to heat stress.<sup>[49]</sup> When *pmk-1* mutants were chronically treated at the stressful temperature (25 °C) we detected a robust reduction of pumping rates upon GO exposure, but not GONH<sub>2</sub> (Figure 3A). Acute treatment at optimal growth temperature marginally reduced the pumping rates but the differences were not statistically significant (Figure S4B, Supporting Information). The *mpk-1* mutant we used carries a temperature sensitive (ts) allele (*ga111*) but when grown at the restrictive temperature of 25 °C we did not detect any effects on the pumping rate upon graphene exposure (Figure 3A). The reduction in pumping rates measured in *pmk-1* mutants chronically exposed to GO at 25 °C went along with morphological decline in the pharyngeal pumping apparatus and the intestine (Figure 3B). Further, the animals developed a severe facultative vivipary (or “bagging”) phenotype, causing internal hatching of the embryos, followed by consuming the parent (Figure S5 (Supporting Information); wild type: control 0%, GO 7.5 ± 5%, GONH<sub>2</sub> 0%; *pmk-1*(km25): control 10 ± 5%, GO 80 ± 10%, GONH<sub>2</sub> 22.5 ± 7.5%;  $n = 25$ ). The size reduction that we had already observed in wild type animals was further enhanced in GO-treated *pmk-1* mutants (Figure 3C). Under the same conditions, we detected a significantly reduced locomotion behavior (Figure S6, Supporting Information). Those phenotypes were significantly less pronounced upon chronic GONH<sub>2</sub> treatment. Conversely, chronic GO treatment at 25 °C did not shorten the lifespan of *pmk-1* mutants below the respective control but led to a slight lifespan extension (2 out of 3 replicates), when bagging animals were censored from the population to begin with. Under the same conditions, the wild type lifespan stayed unaffected from GO or GONH<sub>2</sub> treatment (Figure 3D).

*C. elegans* survival is severely shortened by PA14 exposure, involving an infection-like process when grown on minimal medium (“slow” killing assay).<sup>[50]</sup> On the background of the



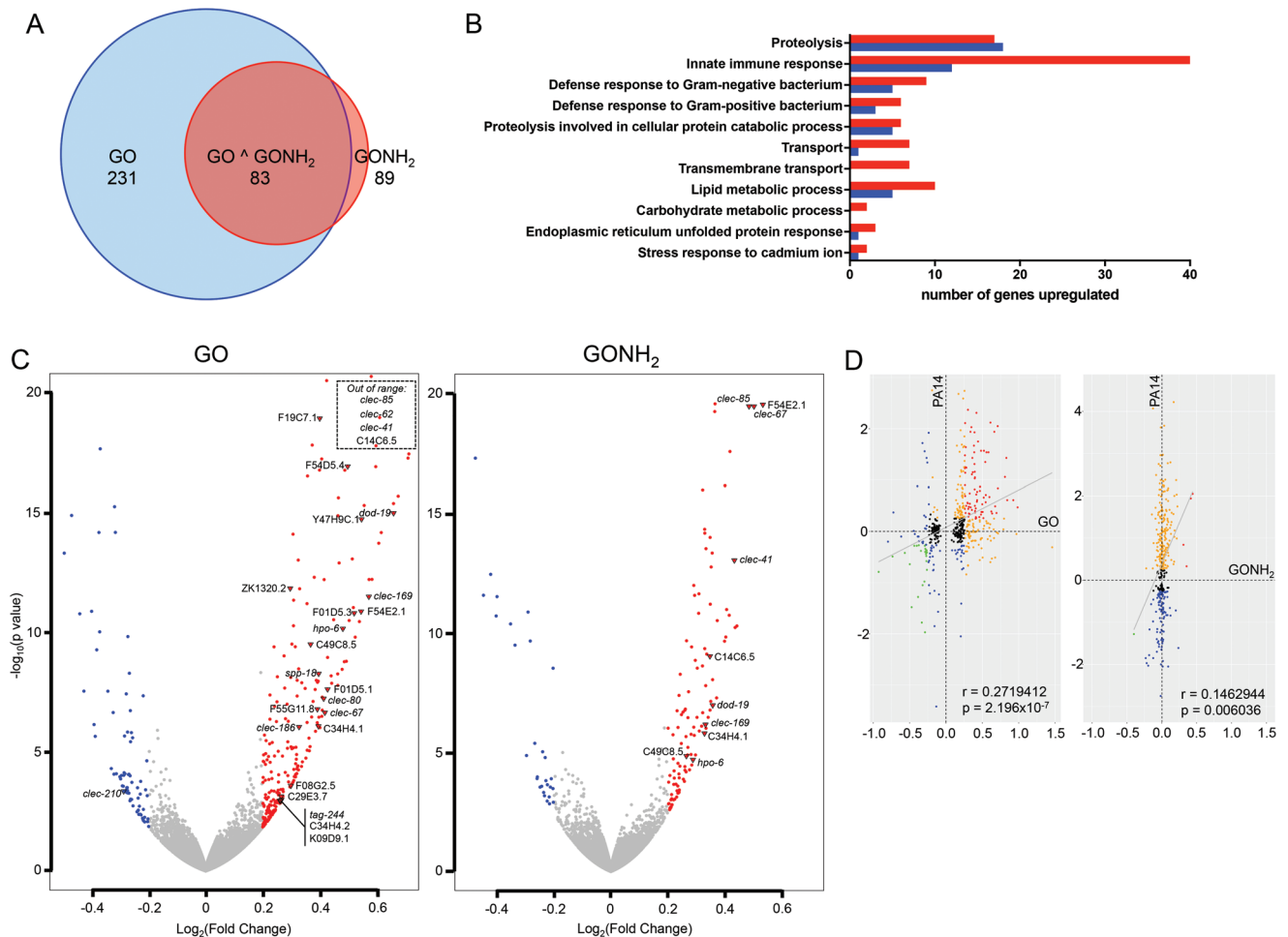


**Figure 2.** Acute treatment leads to a mild induction of genes involved in stress response/innate immunity. A) Venn diagram indicating the total number of genes differentially regulated upon acute GO or GONH<sub>2</sub> exposure at 20 °C. B) Number of genes acting in specific biological processes that are differentially regulated upon acute GO or GONH<sub>2</sub> exposure. C) Volcano blot showing log<sub>2</sub>(FC) of genes that are upregulated (red) or downregulated (blue) with an FC ≥ 1.2, versus the significance of differential regulation given by -log<sub>10</sub>(p value) upon GO or GONH<sub>2</sub> treatment. Genes that act in the innate immune response are labeled (connected Figure S3, Supporting Information). D) Diagram showing the correlation between RNA-Seq data obtained from acutely treated animals with GO (left panel) or GONH<sub>2</sub> (right panel), respectively, with Affymetrix microarray data from animals exposed for 4 h to PA14. Orange, genes upregulated; blue, genes downregulated; red, genes upregulated in both data sets; green, genes downregulated in both data sets; black, genes significantly changed, but below FC ± 1.2. The gray line indicates the correlation between the data sets. The Pearson correlation coefficient and *p*-value for significance of the correlation are indicated in the graph.

elevated innate immune response observed upon GO-treatment we were curious to see whether GO or GONH<sub>2</sub> might alter pathogen-resistance. We found that chronic GO-exposure prior to growth on PA14 decreased *C. elegans* survival on the pathogen, which was not the case upon GONH<sub>2</sub> treatment (Figure 3E; Table S6, Supporting Information). Expectedly, *pmk-1* mutants were more sensitive to PA14 but, surprisingly, were slightly but significantly protected from pathogen infection when pretreated with GO, but not GONH<sub>2</sub> (Figure 3E; Table S6, Supporting Information).

### 2.5. Germline-Less Mutants are Protected from GO Toxicity

The *C. elegans* germline plays an important role in the somatic stress response and longevity.<sup>[51,52]</sup> As mentioned above,

chronic GO treatment leads to a severe bagging phenotype in *pmk-1* mutants (Figure S5, Supporting Information). Bagging negatively affects reproductive fitness and survival of *C. elegans* and is induced when animals are grown in liquid culture, upon starvation conditions, or upon exposure to toxic chemicals or pathogens.<sup>[53–56]</sup> In contrast, laser-assisted germline depletion or genetic mutations that interrupt germ-cell proliferation increase *C. elegans* longevity and the activity of stress response pathways, including resistance to pathogen infection.<sup>[51,57]</sup> We speculated that removal of the germline will avert GO-induced bagging and, consequently, might increase tolerance to graphene toxicity.

To test our hypothesis we crossed *pmk-1* mutants with animals carrying *mpk-1(ga111)* allele, in which germline development and offspring production are impaired when grown at the nonpermissive temperature (25 °C), and determined

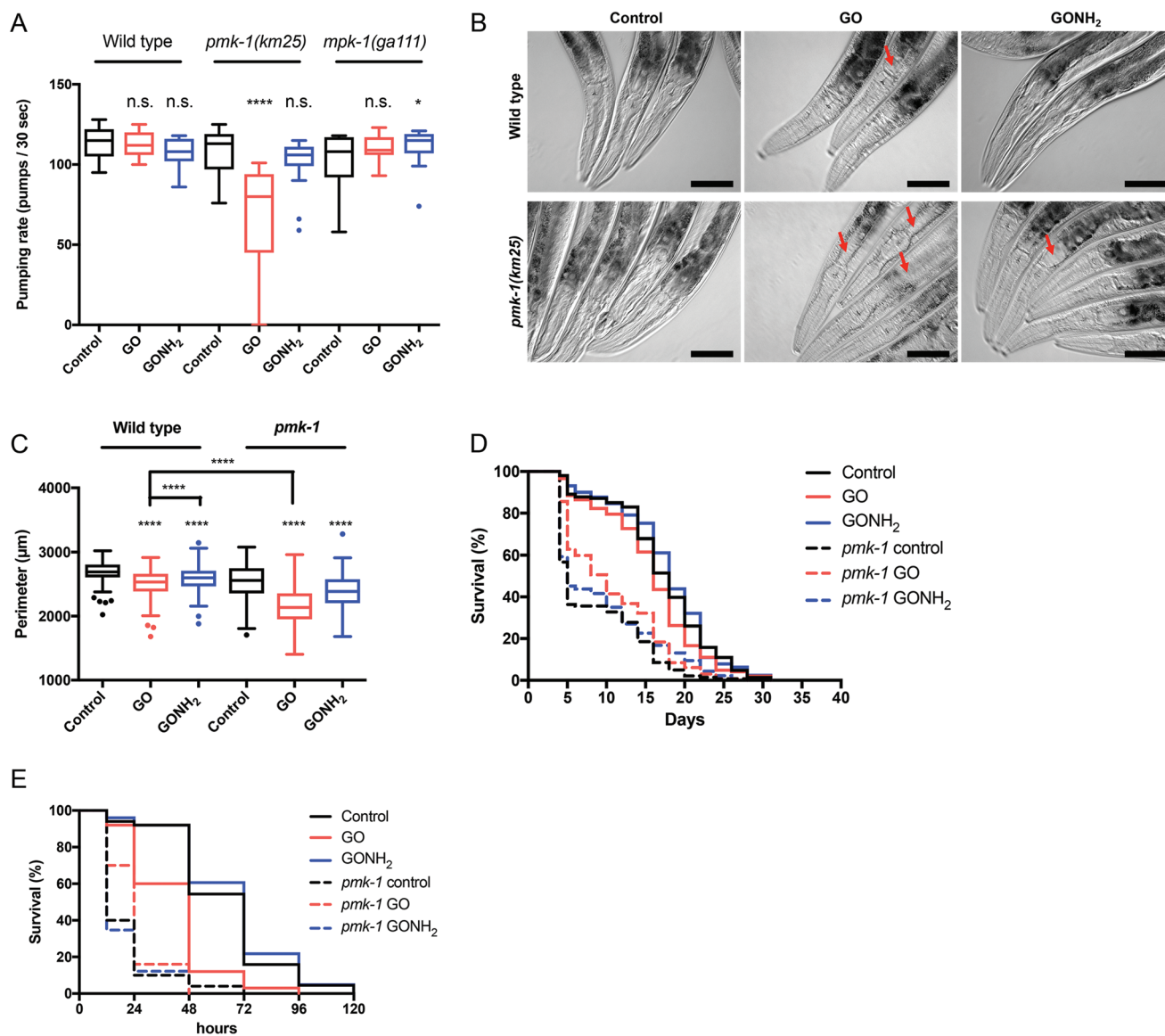


**Figure 3.** Chronic GO treatment affects the physiology of innate immune response defective *pmk-1* mutants. A) Pumping rates measured in wild type, *pmk-1(km25)*, and *mpk-1(ga111)* mutants. Animals were reared at 25 °C (nonpermissive temperature). We used unpaired Mann–Whitney test to analyze the results, with  $****p < 0.0001$  (connected Figure S4, Supporting Information). B) Representative images of the head region of animals after chronic treatment at 25 °C. Red arrows indicate morphological abnormalities in the proximal intestine and pharynx. Size bars correspond to 50  $\mu\text{m}$  (connected Figure S5, Supporting Information). C) Animal size (perimeter) measured upon chronic treatment at 25 °C. Statistical analysis were performed with the Mann–Whitney test with  $**p < 0.01$  and  $****p < 0.0001$ . D) Representative lifespan result of wild type and *pmk-1* mutants (connected Table S1, Supporting Information). E) Representative PA14 pathogen slow killing assay after 72 h of GO or GONH<sub>2</sub> treatment. For statistical analysis compare Table S5 (Supporting Information), which contains the logrank (Mantel–Cox) test and the Gehan–Breslow–Wilcoxon test.

that pharyngeal pumping rates upon chronic GO exposure were unaffected (Figure 4A).<sup>[58]</sup> Similarly, reduced pumping rates upon chronic GO treatment in *pmk-1* mutants were restored to control levels when animals additionally lagged GLP-1, member of the LIN-12/Notch family of receptors that controls germline proliferation (Figure 4B).<sup>[59]</sup> In summary, when germline development and, consequently, offspring production are genetically suppressed, innate immune deficient *pmk-1* mutants display increased tolerance toward GO exposure.

### 3. Conclusion

*C. elegans* has emerged as a powerful model organism to quantitatively assess the molecular mechanisms underlying the toxicity of environmental toxins and nanoparticles.<sup>[27,60,61]</sup> In this study, we measured the adverse effects of GO and GONH<sub>2</sub> upon acute or chronic exposure on various behavioral traits. Fecundity was reduced upon chronic GO exposure, confirming studies in *C. elegans* using GO material based on a different protocol.<sup>[62]</sup> However, the embryonic hatching rate stayed unaffected, while

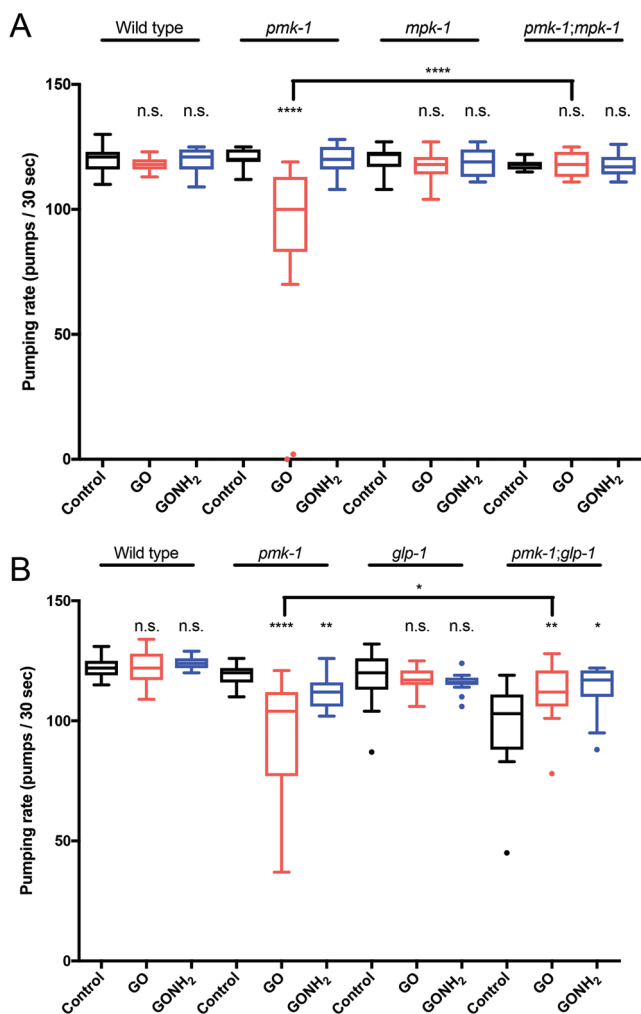


**Figure 4.** Genetic germline depletion protects *pmk-1* mutants from toxic GO effects. A) Pumping rates measured in germline-deficient *pmk-1;mpk-1* double mutants compared to the respective controls. B) Pumping rates of the germline-less *pmk-1;glp-1* double mutants. Both experiments in (A) and (B) were performed at 25 °C (nonpermissive temperature). Mann–Whitney test was used to measure statistical significance, with \* $p < 0.05$ , \*\* $p < 0.01$  and \*\*\*\* $p < 0.0001$ .

facultative vivipary was induced homogeneously throughout a chronically treated population of *pmk-1* mutants. Bagging has been defined as life-history trait in *C. elegans*: it is induced upon environmental stress to ensure the survival of progeny.<sup>[54]</sup> Our treatment paradigm combines stress through elevated temperature (25 °C),<sup>[63]</sup> liquid culture rearing, and graphene exposure in a stress response deficient *pmk-1* mutant, leading to a synergistic toxicity effect that results in severe bagging. Genetic removal of the germline counteracted this deficit, allowing the interpretation that GO might negatively impact on somatic germline development. This could indicate that GO distributes systemically in the animal with the potential of damaging any other cell type, as it has been suggested for GO materials produced via the same method but with different lateral size distribution and chemical functionalization.<sup>[64]</sup>

Chronic GO exposure led to a significantly decreased animal size and we detected morphological abnormalities in the

pharynx and the intestine. Indeed, GO material can penetrate and degrade bacterial and eukaryotic cell membranes, and it has been suggested to breach the *C. elegans* intestinal barrier.<sup>[65–67]</sup> In fact, nematode cells might be particularly susceptible to GO, as they contain a high cholesterol content, and GO has been shown to oxidize cholesterol and to perturb plasma membrane lipid formation.<sup>[19]</sup> Hence, physical damage to the feeding apparatus and the intestine could account for the smaller body size, as reduced food intake and the resulting metabolic changes correlate with decreased animal length.<sup>[68]</sup>

Strikingly, egg-laying and body size were the only parameters that were changed upon chronic exposure, while developmental timing, pharyngeal pumping, locomotion, and lifespan (bagging animals were censored from the population) stayed unaffected, which stands in contrast to previous GO toxicity studies in *C. elegans*.<sup>[34,65,69]</sup> This discrepancy can be explained by differences between the physicochemical characteristics of GO, which has half the lateral size as compared to our study.

Acute treatment did not result in any defects in the measured phenotypes but, curiously, we detected a mobility increase. This trait could be an aversion response, or fight-and-flight response, similarly observed upon exposure to pathogenic bacteria,<sup>[70]</sup> indicating that worms can sense GO material.<sup>[71]</sup> The *C. elegans* intestine acts as a barrier to environmental toxins, metals, nanomaterials or pathogens,<sup>[46,65,72]</sup> and it is instrumental for implementing a systemic innate immune response.<sup>[73]</sup> Our genome-wide RNA-Seq data of acutely GO-treated animals showed an induced expression of innate immune response genes, which significantly, albeit mildly positive correlated with gene expression data obtained from *C. elegans* that encountered pathogenic PA14 bacteria.<sup>[45]</sup> Moreover, we found that animals lacking PMK-1 displayed elevated sensitivity to GO, corroborating previous findings in *C. elegans* that employed different-source GO material.<sup>[74]</sup> We speculated that GO-exposure could immunize *C. elegans* to better tolerate a subsequent lethal pathogen exposure, which would indicate the in vivo outcome of a successfully mounted innate immune response. However, the detrimental effects were additive (Figure 3E), suggesting that GO-exposure causes cellular or organismal stress that goes beyond the defense capacity of innate immune responses. GO has been shown to induce oxidative stress and cytotoxicity in human cells and *C. elegans*, which is attributable to surface-bound endoperoxide groups.<sup>[65,75]</sup>

Overall, our results confirm the notion of previous studies that attribute toxic effects of varying intensity to chronic GO exposure in *C. elegans*, underlining the need for the design of functionalized GO with improved biocompatibility. Previously, we demonstrated that the amino-functionalization of GO changes the impact on human immune cells: while GO triggers an extensive, non-cell-specific cytokine production throughout cell populations, GONH<sub>2</sub> causes a much more specific, polarized Th1 response, which has been implicated in counteracting cancer development.<sup>[26]</sup> In this study, GONH<sub>2</sub> exposure did not cause any measurable detrimental effects in *C. elegans* for the quantified parameters; innate immune induction was considerably lower, and *pmk-1* mutants were not negatively affected by GONH<sub>2</sub>. Curiously, we detected a slight but significant lifespan extension of GONH<sub>2</sub> treated animals. Moderate activation of stress response pathways, including the innate immune

response, can increase cellular stress tolerance and extend health and lifespan through a process called hormesis that has been demonstrated for numerous examples in the nematode.<sup>[76,77]</sup>

In conclusion, we present a comprehensive assessment of GO toxicity in *C. elegans* upon acute or chronic exposure. While the latter causes decreased fecundity and reduced animal size, acute treatment does not result in major health deficits. Our RNA-Seq data resolve that acute exposure to GO triggers an innate immune response that is, in comparison, robustly decreased in GONH<sub>2</sub> treated animals. This study demonstrates the elevated biocompatibility of amino-functionalized GO in a whole-animal context, laying the foundation for future development and convenient in vivo testing of graphene-based nano-medical tools for diagnostics and therapeutics.

#### 4. Experimental Section

**Instruments for GO Characterization:** Thermogravimetric analyses (TGA) were performed on a TGA1 (Mettler Toledo) apparatus from 30 to 900 °C with a ramp of 10 °C min<sup>-1</sup> under N<sub>2</sub> using a flow rate of 50 mL min<sup>-1</sup> and platinum pans. Infrared spectra were recorded using a Nicolet 6700 FT-IR spectrometer (ThermoFisher). The samples were analyzed as dry KBr pellets. XPS analyses were performed on a Thermo Scientific K-Alpha X-ray photoelectron spectrometer with a basic chamber pressure of 10<sup>-8</sup>–10<sup>-9</sup> bar with an anode using Al K<sub>α</sub> radiation ( $h\nu = 1486.6$  eV). The C (1s) photoelectron binding energy was set at 284.5 ± 0.2 eV and used as reference for calibrating the other peak positions. The samples were analyzed as a powder. Spot size of 400 μm was used. The survey spectra are average of 10 scans with a pass-energy of 200.00 eV and a step size of 1 eV. An ion gun was turned on during analysis. For each sample the analysis was repeated three times. TEM images were recorded using a Hitachi 7500 transmission electron microscope (Hitachi High Technologies Corporation, Tokyo, Japan) equipped with an AMT Hamamatsu digital camera (Hamamatsu Photonics, Hamamatsu City, Japan). Samples for AFM measurements were prepared by spin coating GO solutions on freshly cleaned SiO<sub>2</sub>/Si substrates. Images were acquired with a commercial microscope Multimode 8 (Bruker) operated in the tapping mode under ambient conditions. The average size of GO flakes was measured by automatic image processing.<sup>[78]</sup>

**GO Functionalization:** A volume of 77 μL (77 mg, 0.52 mmol) 2,2 (ethylenedioxy)bis(ethylamine) was added under vigorous stirring to 25 mL of a dispersion of GO (1.5 mg mL<sup>-1</sup>, 37.5 mg) in Milli-Q water. The reaction mixture was stirred for 3 d. After centrifugation (5000 rpm, 30 min), the precipitate was dispersed in water and the crude was purified via dialysis against water (Spectra/Por dialysis membrane MWCO 12 000–14 000 Da) for 3 d. The number of amino groups was determined by the Kaiser test.<sup>[38]</sup> This colorimetric test is commonly used in peptide synthesis for the qualitative and quantitative determination of amine functions. The Kaiser test is based on the reaction of amines with ninhydrine, leading to the formation of a chromophoric compound whose concentration can be determined using UV–vis spectroscopy.

***C. elegans* Maintenance:** *C. elegans* strains were maintained and propagated on OP50 *E. coli* seeded nematode growth medium (NGM) at 20 °C according to standard conditions, if not described otherwise.<sup>[79]</sup> The following strains were obtained from *Caenorhabditis* Genetics Center (CGC, Minneapolis, MN, USA): N2, Bristol *C. elegans* wild isolate; KU25 [*pmk-1(km25)* IV]; SD939 [*mpk-1(ga111)* *unc-79(e1068)* III]; CB4037 [*gfp-1(e2141)* IV]; RB911 [*fshr-1(ok778)* V]. The following crosses were used for this study: *pmk-1(km25);mpk-1(ga111);unc-79(e1068)*, *gfp-1(e2144);pmk-1(km25)*.

**Bleach Synchronization of *C. elegans*:** To obtain an L1 stage-synchronized *C. elegans* population, worms and eggs were washed off NGM plates using 5 mL of M9 buffer (3 g KH<sub>2</sub>PO<sub>4</sub>, 6 g Na<sub>2</sub>HPO<sub>4</sub>, 5 g NaCl in ddH<sub>2</sub>O, autoclaved, then supplemented with 1 × 10<sup>-3</sup> M

MgSO<sub>4</sub>). Worms were gently scraped off the plates with cell scrapers (VWR) and transferred into 15 mL centrifuge tubes (Falcon). Then 1 mL bleaching solution (5 M NaOH, sodium hypochloride solution ≈10%, 1:1 mixture, Aldrich) was added and incubated for 5 min while continuously vortexing. Worms were then washed three times by centrifugation at 2800 rpm for 1 min at 20 °C (Centrifuge 5810R, Eppendorf) and replacing the supernatant with fresh M9 buffer. After the last washing step, ampicillin (stock solution 100 mg mL<sup>-1</sup> in H<sub>2</sub>O) was added to the M9 buffer in a 1:1000 ratio. Eggs were incubated in 15 mL centrifuge tubes overnight (16–17 h) at room temperature (RT) on a rotating mixer (35 rpm) and hatched animals were pelleted the next day by centrifugation for 1 min at 1300 rpm. After removing the supernatant to about 1 mL, the number of hatched animals in a representative volume (3 μL) was determined at a Stereomicroscope (Leica M80).

**Acute and Chronic GO Exposure in Liquid Culture:** The L1 staged populations were pelleted by centrifugation at 1300 rpm for 1 min and resuspended in 2 mL K-medium (2.36 g KCl, 3 g NaCl in 1 L ddH<sub>2</sub>O, autoclaved). The wells of a 24-well plate were prepared by adding 100 μL of a 1:250 suspension of cholesterol (5 mg mL<sup>-1</sup> in EtOH) in sterile K-Medium (cholesterol is part of the standard *C. elegans* growth medium, as nematodes are auxotrophic for sterols), 100 μL of 50× concentrated *E. coli* OP50 culture with an OD of 0.9, pelleted by centrifugation (Centrifuge 5810R, Eppendorf) and resuspended in K-Medium, and 200 μL K-Medium. A volume of GO or GONH<sub>2</sub> suspension in ddH<sub>2</sub>O was added to a final concentration of 100 μg mL<sup>-1</sup> solution per well as the experimental standard condition, while no material was added to the control wells. An adjusted volume containing 300–400 worms suspended in K-medium was then added, bringing the final volume to 400 μL per well. Experiments were set up in triplicates per strain and condition. Unused wells were filled up with ddH<sub>2</sub>O and the 24-well plate was sealed with parafilm and placed in a closed plastic box together with wet paper towels to prevent the wells from drying out during prolonged incubation periods. For chronic treatments, animals were incubated for 72 h at the standard *C. elegans* culturing temperature of 20–22 °C, or at 25 °C, while shaking at 120 rpm. For the acute treatment, synchronized L1-larvae populations were grown on NGM plates seeded with OP50 into the L4 larval stage, then rinsed with K-Medium into a 15 mL Falcon tube (≈60 h after seeding), washed in K-Medium by letting the worms settle through gravity and removing the supernatant, and finally the suspension volume was adjusted to 2 mL with K-Medium. After determination of animal density by drop counting at the stereomicroscope, 300–400 animals were added to each well and incubated at 20–22 °C for 12 h while shaking at 120 rpm. After acute or chronic exposure, animals were washed once, transferred to OP50 seeded NGM plates, and allowed to recover for 4 h. Worms were then picked from these plates for further assays and toxicity assessments.

**Egg laying and Hatching Rate Assay:** To assess fertility upon graphene treatment, three gravid adult worms were transferred to OP50 seeded NGM plates and allowed to lay eggs for 3 h (in quadruplets). Then the adults were removed and eggs were counted right after. The hatching rate of the laid eggs was determined by counting the larvae 24 h later.

**Quantification of Development Stages:** The worms were screened for developmental defects after graphene treatment by transferring about 100 individuals per strain to separate 3.5 cm OP50 seeded NGM plates. Representative Images were taken of each plate at 14-fold magnification using an Axio Zoom-V16 Stereomicroscope with camera at the indicated time points (12, 48, and 72 h after treatment). The number of worms on each plate of was determined in silico by using the “Cell Counter” plugin (written by Kurt De Vos, University of Sheffield, Academic Neurology) implemented in the ImageJ software.

**Pharyngeal Pumping Rate Assay:** 20 worms per strain and treatment condition were transferred to a fresh OP50 seeded NGM plate and pumping rates were measured by counting pharyngeal contraction in 30 s timeframes using a high-resolution Stereomicroscope (Zeiss, Axio Zoom-V16).

**Locomotion Assay:** About 50–100 worms per strain and treatment condition were transferred to an OP50 seeded NGM plate. Movements of the worms were recorded for 30 s with 14 frames s<sup>-1</sup> using an Axio



Zoom-V16 Stereomicroscope with camera at tenfold magnification. Average and maximum movement speed, distance covered by animal from start to finish, sum of length of all movement vectors, and length of the average perimeter (outline) of each recorded worm were assessed using the “wrMTrck” plugin implemented in the ImageJ software.<sup>[41]</sup> Data were averaged and plotted for each strain and condition.

**Lifespan Assay:** Lifespan was assessed starting at young adult stage after recovery from liquid GO or GONH<sub>2</sub> treatment. 150 healthy worms that did not display a bagging phenotype, per strain and condition, were equally distributed on 10 OP50 seeded NGM plates and scored for death events at least every second day until all worms were dead. Worms were transferred to fresh OP50 seeded NGM plates at each scoring time point during their fertile lifespan. Animals were censored if I) they could not be localized, II) died after crawling off the agar surface or immersed into the agar, or III) displayed bagging. All death events over time for each strain and condition were summarized in a final lifespan curve and statistics were performed through the Graphpad Prism software.

**RNA Isolation for RT-qPCR and RNA-Seq:** Total RNA for RT-qPCR was extracted from 100 worms per strain and condition, and for RNA-Seq from 500 worms per strain and condition, after 4 h of recovery following liquid culture. Worms were transferred into 50 µL M9 buffer, subsequently 1 mL Trizol was added and the solution was frozen at -80 °C. Samples were then thawed, transferred into homogenizer vials (Peqlab/VWR, 91-PCS-TV and 91-PCS-TC) filled up to 0.5 cm with beads (Zirconia/Glas-Beads, Carl Roth) and homogenized at 6000 rpm for two times 20 s with 30 s pause using a Precellys Lyser (Peqlab). After 5 min of incubation at RT, 100 µL BCP was added and samples vortexed for 15 s, followed by 2 min incubation at RT. Samples were centrifuged for 15 min at 12 000 rcf at 4 °C and upper clear phase was transferred into a new 1.5 mL reaction tube. RNA was isolated using the Qiagen RNeasy Mini Kit (Qiagen), eluted in 30 µL RNase free H<sub>2</sub>O, and processed for RNA-Seq with an Illumina HiSeq4000. For reverse-transcription, RNA was diluted to 1 µg in 11.5 µL total volume, incubated at 70 °C for 2 min and subsequently chilled on ice. For cDNA synthesis, 8.5 µL reverse-transcription master mix (4 µL 5× First-Strand Buffer [Invitrogen], 2 µL 0.1 M DTT [Invitrogen], 1 µL dNTPs, 1 µL 50 × 10<sup>-6</sup> M oligo dTs [Invitrogen], 0.5 µL Superscript III RT enzyme [Invitrogen]) was added to each sample and incubated for 1.5 h at 42 °C followed by 5 min incubation at 92 °C. To adjust the cDNA volume to 100 µL, 80 µL ddH<sub>2</sub>O was added and the cDNA was directly used for qPCR or stored at -20 °C. Real-time qPCR was performed using Platinum Taq (Invitrogen) for amplification and SYBR Green (Sigma Aldrich) for detection. Reactions were carried out in 96-well qPCR plates (Bioplastics) covered with plate sealing film (Biorad). Real-time qPCR was run at the optimized annealing temperature of 58 °C. Used primers for target and reference genes are listed in Table S5 (Supporting Information). All reactions were performed in triplicate. Relative quantification of each of three target gene replicate in comparison to each of three replicates of five reference genes was determined and with the obtained values the averaged ratios between target gene and reference gene expression were calculated considering all 5 reference genes.

**RNA-Seq Data Analysis:** The data files were deposited under the GEO accession code GSE131070. Data were processed through the QuickNGS pipeline,<sup>[80]</sup> Ensembl version 93. Reads were mapped to the *C. elegans* genome using Tophat (version 2.0.10) and abundance estimation was performed with Cufflinks (Version 2.1.1). DESeq2 was used for differential gene expression analysis. The results were uploaded into the QuickNGS database. Microarray data was analyzed by using Affymatrix Power Tools (version 1.15.1), which was applied to subtract the background, normalization and summarizing expression probe data from the CEL files. To calculate the differential expression and the *q* values, R-packages were used, including ggplot2 for the correlation analysis between RNA-Seq and Affymatrix data.

**Slow Killing Assay:** Four days before assay start *Pseudomonas aeruginosa* strain PA14 was freshly streaked from a frozen stock on LB agar, incubated at 37 °C for 12–18 h overnight and subsequently shifted to 4 °C. Two days before the assay start 15 mL LB liquid medium was inoculated with a PA14 colony and incubated for 12–16 h overnight.

The same day, slow killing plates were prepared by mixing 3.5 g Bacto-Peptone, 3 g NaCl, and 17 g Bacto(Serva)-Agar in 1 L ddH<sub>2</sub>O, autoclaving, adding of 1 mL 1 M MgSO<sub>4</sub>, 25 mL 1 M KH<sub>2</sub>PO<sub>4</sub> (pH 6), 1 mL of 1 M CaCl<sub>2</sub>, and 1 mL of 5 mg mL<sup>-1</sup> cholesterol in ethanol after the medium was chilled to 55 °C and subsequently SK medium was poured into 3.5 cm sterile Petri dishes. Plates were stored at 4 °C after drying at RT overnight. One day before assay start, 10 µL of overnight grown PA14 culture was added to each SK plate and spread into ≈1 cm<sup>2</sup> squares in the middle of the plates using a sterile cell scraper. PA14 seeded SK plates were left to dry at RT for 20 min before incubation at 37 °C for 24 h. To start the experiment, 40 pretreated worms were picked on an SK plate and shifted to 25 °C. The experiment was set up in triplicates and scored at the indicated time points. Censoring was performed according to the lifespan assay protocol. Surviving animals were transferred to the empty PA14 seeded SK plates in a 24 h rhythm to avoid crowding by the offspring population.

## Supporting Information

Supporting Information is available from the Wiley Online Library or from the author.

## Acknowledgements

The authors thank Najmeh Soltanmohammadi and Flavia Ribezzo for preparing the *mpk-1;pmk-1* and *glp-1;pmk-1* double-mutant strains. The authors also thank Drs. Andrea Liscio and Andrea Candini for helping with the AFM analysis. The authors thank C. Royer and V. Demais for TEM analysis at the “Plateforme Imagerie in Vitro” at the Center of Neurochemistry (INCI, Strasbourg, France). The authors gratefully acknowledge financial support from ANR (ANR-15-GRFL-0001-05), MIUR JTC Graphene 2015 (G-IMMUNOMICS project), and European Union HORIZON 2020 research and Graphene Flagship project (no. 785219). This work was partly supported by the Centre National de la Recherche Scientifique (CNRS), the Agence Nationale de la Recherche (ANR) through the LabEx project Chemistry of Complex Systems (ANR-10-LABX-0026\_CSC), and the International Center for Frontier Research in Chemistry (icFRC). B.S. acknowledges funding from the Deutsche Forschungsgemeinschaft (SCHU 2494/3-1, SCHU 2494/7-1, CECAD, SFB 829, SFB 670, KFO 286, and KFO 329), the Deutsche Krebshilfe (70112899), and the COST action (BM1408, GENIE).

Note: A typo in the author Lucia Gemma Delogu's name was corrected and the 7th affiliation was added on 6 November 2019 after original online publication.

## Conflict of Interest

The authors declare no conflict of interest.

## Keywords

amino-functionalized graphene oxide, *Caenorhabditis elegans*, graphene oxide, innate immunity

Received: May 24, 2019  
Revised: August 29, 2019  
Published online: October 1, 2019

[1] G. A. Silva, *Nat. Rev. Neurosci.* **2006**, *7*, 65.

[2] D. A. Scheinberg, C. H. Villa, F. E. Escorcia, M. R. McDevitt, *Nat. Rev. Clin. Oncol.* **2010**, *7*, 266.

- [3] A. K. Geim, K. S. Novoselov, *Nat. Mater.* **2007**, *6*, 183.
- [4] K. S. Novoselov, V. I. F. ko, L. Colombo, P. R. Gellert, M. G. Schwab, K. Kim, *Nature* **2012**, *490*, 192.
- [5] K. S. Novoselov, A. K. Geim, S. V. Morozov, D. Jiang, Y. Zhang, S. V. Dubonos, I. V. Grigorieva, A. A. Firsov, *Science* **2004**, *306*, 666.
- [6] S. R. Shin, Y.-C. Li, H. L. Jang, P. Khoshakhlagh, M. Akbari, A. Nasajpour, Y. S. Zhang, A. Tamayol, A. Khademhosseini, *Adv. Drug Delivery Rev.* **2016**, *105*, 255.
- [7] J. Tian, Y. Luo, L. Huang, Y. Feng, H. Ju, B.-Y. Yu, *Biosens. Bioelectron.* **2016**, *80*, 519.
- [8] H. Dong, W. Dai, H. Ju, H. Lu, S. Wang, L. Xu, S.-F. Zhou, Y. Zhang, X. Zhang, *ACS Appl. Mater. Interfaces* **2015**, *7*, 11015.
- [9] S. K. Maji, A. K. Mandal, K. T. Nguyen, P. Borah, Y. Zhao, *ACS Appl. Mater. Interfaces* **2015**, *7*, 9807.
- [10] N. F. Rosli, M. Fojtů A. C. Fisher, M. Pumera, *Langmuir* **2019**, *35*, 3176.
- [11] E. Campbell, M. T. Hasan, C. Pho, K. Callaghan, G. R. Akkaraju, A. V. Naumov, *Sci. Rep.* **2019**, *9*, 416.
- [12] J. Russier, V. León, M. Orecchioni, E. Hirata, P. Virdis, C. Fozza, F. Sgarrella, G. Cuniberti, M. Prato, E. Vázquez, A. Bianco, L. G. Delogu, *Angew. Chem., Int. Ed.* **2017**, *56*, 3014.
- [13] M. Orecchioni, C. Ménard-Moyon, L. G. Delogu, A. Bianco, *Adv. Drug Delivery Rev.* **2016**, *105*, 163.
- [14] B. Fadeel, C. Bussy, S. Merino, E. Vázquez, E. Flahaut, F. Mouchet, L. Evariste, L. Gauthier, A. J. Koivisto, U. Vogel, C. Martín, L. G. Delogu, T. Buerki-Thurnherr, P. Wick, D. Beloin-Saint-Pierre, R. Hirschier, M. Pelin, F. Candotto Carniel, M. Tretiach, F. Cesca, F. Benfenati, D. Scaini, L. Ballerini, K. Kostarelos, M. Prato, A. Bianco, *ACS Nano* **2018**, *12*, 10582.
- [15] E. Hashemi, O. Akhavan, M. Shamsara, M. Daliri, M. Dashtizad, A. Farmany, *Colloids Surf., B* **2016**, *146*, 770.
- [16] S. Liang, S. Xu, D. Zhang, J. He, M. Chu, *Nanotoxicology* **2015**, *9*, 92.
- [17] X. Wang, R. Podila, J. H. Shannahan, A. M. Rao, J. M. Brown, *Int. J. Nanomed.* **2013**, *8*, 1733.
- [18] A. Schinwald, F. A. Murphy, A. Jones, W. MacNee, K. Donaldson, *ACS Nano* **2012**, *6*, 736.
- [19] S. P. Mukherjee, B. Lazzaretto, K. Hultenby, L. Newman, A. F. Rodrigues, N. Lozano, K. Kostarelos, P. Malmberg, B. Fadeel, *Chem* **2018**, *4*, 334.
- [20] M. Ema, M. Gamo, K. Honda, *Regul. Toxicol. Pharmacol.* **2017**, *85*, 7.
- [21] F. M. Tonelli, V. A. Goulart, K. N. Gomes, M. S. Ladeira, A. K. Santos, E. Lorençon, L. O. Ladeira, R. R. Resende, *Nanomedicine* **2015**, *10*, 2423.
- [22] P. Wick, A. E. Louw-Gaume, M. Kucki, H. F. Krug, K. Kostarelos, B. Fadeel, K. A. Dawson, A. Salvati, E. Vázquez, L. Ballerini, M. Tretiach, F. Benfenati, E. Flahaut, L. Gauthier, M. Prato, A. Bianco, *Angew. Chem., Int. Ed.* **2014**, *53*, 7714.
- [23] H. Asgar, K. M. Deen, Z. U. Rahman, U. H. Shah, M. A. Raza, W. Haider, *Mater. Sci. Eng., C* **2019**, *94*, 920.
- [24] F. Liu, D. Yang, Y. Liu, Q. Cao, Y. Sun, Q. Wang, H. Tang, *Colloids Surf., B* **2018**, *171*, 622.
- [25] A. Sasidharan, L. S. Panchakarla, A. R. Sadanandan, A. Ashokan, P. Chandran, C. M. Girish, D. Menon, S. V. Nair, C. N. R. Rao, M. Koyakutty, *Small* **2012**, *8*, 1251.
- [26] M. Orecchioni, D. Bedognetti, L. Newman, C. Fuoco, F. Spada, W. Hendrickx, F. M. Marincola, F. Sgarrella, A. F. Rodrigues, C. Ménard-Moyon, G. Cesareni, K. Kostarelos, A. Bianco, L. G. Delogu, *Nat. Commun.* **2017**, *8*, 1109.
- [27] S.-K. Jung, X. Qu, B. Aleman-Meza, T. Wang, C. Riepe, Z. Liu, Q. Li, W. Zhong, *Environ. Sci. Technol.* **2015**, *49*, 2477.
- [28] T. Kaletta, M. O. Hengartner, *Nat. Rev. Drug Discovery* **2006**, *5*, 387.
- [29] M. Artal-Sanz, L. de Jong, N. Tavernarakis, *Biotechnol. J.* **2006**, *1*, 1405.
- [30] M. A. Ermolaeva, B. Schumacher, *Semin. Immunol.* **2014**, *26*, 303.
- [31] M. Rodriguez, L. B. Snoek, M. De Bono, J. E. Kammenga, *Trends Genet.* **2013**, *29*, 367.
- [32] E. Zanni, G. De Bellis, M. P. Bracciale, A. Broggi, M. L. Santarelli, M. S. Sarto, C. Palleschi, D. Uccelletti, *Nano Lett.* **2012**, *12*, 2740.
- [33] W. Zhang, C. Wang, Z. Li, Z. Lu, Y. Li, J.-J. Yin, Y.-T. Zhou, X. Gao, Y. Fang, G. Nie, Y. Zhao, *Adv. Mater.* **2012**, *24*, 5391.
- [34] Y. Zhao, R. Yang, Q. Rui, D. Wang, *Sci. Rep.* **2016**, *6*, 24024.
- [35] N. Chatterjee, J. S. Yang, K. Park, S. M. Oh, J. Park, J. Choi, *Environ. Health Toxicol.* **2015**, *30*, e2015007.
- [36] E. Treossi, M. Melucci, A. Liscio, M. Gazzano, P. Samori, V. Palermo, *J. Am. Chem. Soc.* **2009**, *131*, 15576.
- [37] N. Do Quyen Chau, G. Reina, J. Raya, I. A. Vacchi, C. Ménard-Moyon, Y. Nishina, A. Bianco, *Carbon* **2017**, *122*, 643.
- [38] I. A. Vacchi, C. Spinato, J. Raya, A. Bianco, C. Ménard-Moyon, *Nanoscale* **2016**, *8*, 13714.
- [39] J. E. Kimble, J. G. White, *Dev. Biol.* **1981**, *81*, 208.
- [40] M. Rieckher, A. Bujarrabal, M. A. Doll, N. Soltanmohammadi, B. Schumacher, *J. Cell. Physiol.* **2018**, *233*, 2781.
- [41] C. I. Nussbaum-Krammer, M. F. Neto, R. M. Brielmann, J. S. Pedersen, R. I. Morimoto, *J. Visualized Exp.* **2015**, *7*, 52321.
- [42] L. Avery, H. R. Horvitz, *J. Exp. Zool.* **1990**, *253*, 263.
- [43] M. S. Denzel, L. R. Lapierre, H. I. D. Mack, *Mech. Ageing Dev.* **2019**, *177*, 4.
- [44] R. Pukkila-Worley, *PLoS Pathog.* **2016**, *12*, e1005795.
- [45] E. R. Troemel, S. W. Chu, V. Reinke, S. S. Lee, F. M. Ausubel, D. H. Kim, *PLoS Genet.* **2006**, *2*, e183.
- [46] D. H. Kim, R. Feinbaum, G. Alloing, F. E. Emerson, D. A. Garsin, H. Inoue, M. Tanaka-Hino, N. Hisamoto, K. Matsumoto, M.-W. Tan, F. M. Ausubel, *Science* **2002**, *297*, 623.
- [47] H. R. Nicholas, J. Hodgkin, *Curr. Biol.* **2004**, *14*, 1256.
- [48] J. R. Powell, D. H. Kim, F. M. Ausubel, *Proc. Natl. Acad. Sci. USA* **2009**, *106*, 2782.
- [49] A. Mertensköter, A. Keshet, P. Gerke, R. J. Paul, *Cell Stress Chaperones* **2013**, *18*, 293.
- [50] M. W. Tan, S. Mahajan-Miklos, F. M. Ausubel, *Proc. Natl. Acad. Sci. USA* **1999**, *96*, 715.
- [51] H. Hsin, C. Kenyon, *Nature* **1999**, *399*, 362.
- [52] N. Arantes-Oliveira, J. Apfeld, A. Dillin, C. Kenyon, *Science* **2002**, *295*, 502.
- [53] D. R. Shook, T. E. Johnson, *Genetics* **1999**, *153*, 1233.
- [54] J. Chen, E. P. Caswell-Chen, *J. Nematol.* **2004**, *36*, 107.
- [55] J. M. Van Raamsdonk, S. Hekimi, *PLoS Genet.* **2009**, *5*, e1000361.
- [56] T. Mosser, I. Matic, M. Leroy, *Appl. Environ. Microbiol.* **2011**, *77*, 8189.
- [57] S. Alper, M. K. McElwee, J. Apfeld, B. Lackford, J. H. Freedman, D. A. Schwartz, *J. Biol. Chem.* **2010**, *285*, 1822.
- [58] M.-H. Lee, M. Ohmachi, S. Arur, S. Nayak, R. Francis, D. Church, E. Lambie, T. Schedl, *Genetics* **2007**, *177*, 2039.
- [59] J. Austin, J. Kimble, *Cell* **1987**, *51*, 589.
- [60] J. Choi, O. V. Tsyusko, J. M. Unrine, N. Chatterjee, J.-M. Ahn, X. Yang, B. L. Thornton, I. T. Ryde, D. Starnes, J. N. Meyer, *Environ. Chem.* **2014**, *11*, 227.
- [61] N. Shin, L. Cuenca, R. Karthikraj, K. Kannan, M. P. Colaiácovo, *PLoS Genet.* **2019**, *15*, e1007975.
- [62] Y. Zhao, Q. Wu, D. Wang, *Biomaterials* **2016**, *79*, 15.
- [63] D. Y. Gouvêa, E. Z. Aprison, I. Ruvinsky, *PLoS One* **2015**, *10*, e0145925.
- [64] Q. Wu, Y. Zhao, J. Fang, D. Wang, *Nanoscale* **2014**, *6*, 5894.
- [65] Q. Wu, L. Yin, X. Li, M. Tang, T. Zhang, D. Wang, *Nanoscale* **2013**, *5*, 9934.
- [66] C. Sun, D. L. Wakefield, Y. Han, D. A. Muller, D. A. Hlowka, B. A. Baird, W. R. Dichtel, *Chem* **2016**, *1*, 273.
- [67] Y. Tu, M. Lv, P. Xiu, T. Huynh, M. Zhang, M. Castelli, Z. Liu, Q. Huang, C. Fan, H. Fang, R. Zhou, *Nat. Nanotechnol.* **2013**, *8*, 594.

- [68] C. Mörck, M. Pilon, *BMC Dev. Biol.* **2006**, *6*, 39.
- [69] Q. Wu, Y. Zhao, Y. Li, D. Wang, *Nanoscale* **2014**, *6*, 11204.
- [70] J. Singh, A. Aballay, *Dev. Cell* **2019**, *49*, 89.
- [71] G. Xiao, H. Chen, N. Krasteva, Q. Liu, D. Wang, *J. Nanobiotechnol.* **2018**, *16*, 45.
- [72] B. Vigneshkumar, S. K. Pandian, K. Balamurugan, *Environ. Toxicol.* **2013**, *28*, 313.
- [73] H. Schulenburg, C. L. Kurz, J. J. Ewbank, *Immunol. Rev.* **2004**, *198*, 36.
- [74] Y. Zhao, L. Zhi, Q. Wu, Y. Yu, Q. Sun, D. Wang, *Nanotoxicology* **2016**, *10*, 1469.
- [75] H. Pieper, S. Chercheja, S. Eigler, C. E. Halbig, M. R. Filipovic, A. Mokhir, *Angew. Chem., Int. Ed.* **2016**, *55*, 405.
- [76] N. Kourtis, N. Tavernarakis, *EMBO J.* **2011**, *30*, 2520.
- [77] E. Yunger, M. Safra, M. Levi-Ferber, A. Haviv-Chesner, S. Henis-Korenblit, *PLoS Genet.* **2017**, *13*, e1006577.
- [78] A. Liscio, K. Kouroupis-Agalou, X. D. Betriu, A. Kovtun, E. Treossi, N. M. Pugno, G. De Luca, L. Giorgini, V. Palermo, *2D Mater.* **2017**, *4*, 025017.
- [79] S. Brenner, *Genetics* **1974**, *77*, 71.
- [80] P. Wagle, M. Nikolic', P. Frommolt, *BMC Genomics* **2015**, *16*, 487.